
LIGHTONOCR: A 1B END-TO-END MULTILINGUAL VISION-LANGUAGE MODEL FOR STATE-OF-THE-ART OCR

Said Taghadouini Adrien Cavaillès Baptiste Aubertin
LightOn

ABSTRACT

We present **LightOnOCR-2-1B**, a 1B-parameter end-to-end multilingual vision–language model that converts document images (e.g., PDFs) into clean, naturally ordered text without brittle OCR pipelines. Trained on a large-scale, high-quality distillation mix with strong coverage of scans, French documents, and scientific PDFs, LightOnOCR-2 achieves state-of-the-art results on OlmOCR-Bench while being $9\times$ smaller and substantially faster than prior best-performing models. We further extend the output format to predict normalized bounding boxes for embedded images, introducing localization during pretraining via a resume strategy and refining it with RLVR using IoU-based rewards. Finally, we improve robustness with checkpoint averaging and task-arithmetic merging. We release model checkpoints under Apache 2.0, and publicly release the dataset and **LightOnOCR-bbox-bench** evaluation under their respective licenses.

Model: <https://huggingface.co/collections/lightonai/lightonocr-2>
Blog: <https://huggingface.co/blog/lightonai/lightonocr-2>
Benchmark: <https://huggingface.co/datasets/lightonai/LightOnOCR-bbox-bench>

1 Introduction

Despite decades of progress in Optical Character Recognition (OCR), from classical engines such as Tesseract [1], to deep neural sequence recognizers like CRNN [2], and Transformer-based models such as TrOCR [3], real-world documents remain challenging: reading order can be ambiguous in multi-column layouts, tables require consistent structure, and scientific PDFs often mix dense typography with mathematical notation, figures, and noisy scans. A common production strategy is to rely on multi-stage pipelines (e.g., layout analysis, text detection, text recognition, table extraction, and reading-order reconstruction), as in systems such as PaddleOCR [4, 5] and MinerU [6]. While effective in many settings, these pipelines couple multiple components and intermediate representations, making them costly to adapt: improving performance on a new document distribution often requires additional annotations for intermediate tasks (layout regions, table structure, reading order) and coordinated changes across stages.

End-to-end vision-language models (VLMs) reduce this engineering burden by learning extraction directly from pixels to structured text [7, 8, 9, 10, 11, 12]. This enables continuous improvement and specialization via straightforward fine-tuning, without retooling each stage of a pipeline. In this work, we present **LightOnOCR-2**, a compact 1B-parameter end-to-end multilingual VLM that achieves state-of-the-art OCR, outperforming substantially larger systems, and extends OCR with document image localization through predicted bounding boxes.

In this context, we release LightOnOCR, a compact, end-to-end model that delivers state-of-the-art document understanding with lightning speed and low cost. Competing systems(including newest releases) often rely on multiple moving parts to boost performance, but this added complexity makes them brittle, difficult to train, and prone to break when adapting to new data or domains. LightOnOCR, on the other hand, is a single unified model — fully differentiable and easy to optimize end-to-end — capable of handling complex layouts such as tables, forms, receipts, and scientific notation without fragile multi-stage pipelines.

LightOnOCR-2-1B is a compact, end-to-end model that builds on our first release [13] with a substantially expanded and cleaner training mixture ($2.5\times$ larger), with increased coverage of scans, French documents, and scientific content, supported by an improved data curation pipeline. During pretraining, we train at higher resolution (maximum longest

edge 1540px), apply data augmentation, and explicitly include empty pages to reduce looping behaviors and improve full-page fidelity. We then apply Reinforcement Learning with Verifiable Rewards (RLVR) [14] to target persistent failure modes that are difficult to address with supervised learning alone, including repetition loops, math rendering and formatting errors, and layout-sensitive consistency constraints enforced through unit-test style checks. We also train a variant to predict bounding boxes for embedded images. To avoid degrading OCR quality with naive supervised fine-tuning, we introduce coordinate supervision during pretraining via a resume strategy and then refine localization using RLVR with IoU-based objectives. Finally, we leverage lightweight weight-space techniques, checkpoint averaging and task-arithmetic merging, to combine complementary gains and to control the trade-off between OCR quality and bounding box (bbox) accuracy.

Contributions To summarize, we make the following contributions:

- We release **LightOnOCR-2-1B**, a compact 1B-parameter end-to-end multilingual VLM for document parsing that achieves a new state-of-the-art result on OlmOCR-Bench, outperforming substantially larger models (e.g., 9B-scale baselines).
- We scale and improve the pretraining mixture ($2.5 \times$ larger) with stronger coverage of French and scientific documents, higher-resolution training (max longest edge 1540px), improved normalization (cleaner \LaTeX handling), and robustness via data augmentations and explicit empty-page targets.
- We introduce a `nvpdftex`-based arXiv curation pipeline to obtain pixel-aligned supervision from \TeX sources, and use it both to strengthen scientific OCR supervision and to generate an automatic subset for our localization benchmark.
- We add image bounding box prediction in dedicated variants by introducing coordinate supervision during pretraining and refining localization with RLVR using IoU-based objectives.
- We introduce **LightOnOCR-bbox-bench**, a new benchmark for image localization in documents.
- We show that lightweight weight-space techniques, checkpoint averaging and task-arithmetic merging, can improve OCR and enable controlled trade-offs between OCR quality and bbox accuracy across released checkpoints.

2 Overview

In this section, we describe the LightOnOCR architecture and summarize the training recipe differences between LightOnOCR-1B and LightOnOCR-2-1B.

2.1 Architecture

LightOnOCR is a compact 1B-parameter vision-language model composed of three main components: a vision encoder, a multimodal projector, and a language model decoder. We train the model to perform OCR without task prompts at inference time, so the extraction behavior is embedded in the weights rather than controlled by an explicit prompt.

Vision Encoder We employ a native-resolution Vision Transformer initialized from the pretrained `Mistral-Small-3.1` [15] vision encoder weights. This encoder handles variable image sizes while preserving spatial structure, which is critical for documents with diverse aspect ratios and fine typographic details.

Multimodal Projector To bridge the vision and language modalities while controlling sequence length, we use a two-layer MLP with GELU activation that projects vision features into the language model’s embedding space. Before projection, we apply spatial merging with a factor of 2, effectively grouping 2×2 patches and reducing the number of visual tokens by $4 \times$. This keeps the overall token count tractable for high-resolution inputs while preserving sufficient spatial granularity. The projector is randomly initialized and trained from scratch.

Language Model Decoder We initialize the decoder from pretrained `Qwen3` [16]. The decoder produces a single, linearized representation of the page that preserves reading order while emitting structured tokens for non-text elements (e.g., `! [image] (image_N.png)`). To simplify the interface between modalities, we remove the image-break and image-end tokens and condition the decoder on a single contiguous block of visual tokens (after spatial merging), followed by text tokens. This yields a compact end-to-end VLM with a consistent generation format across datasets.

Initialization By initializing from strong pretrained components, LightOnOCR inherits robust visual representations and multilingual language modeling capabilities, enabling effective transfer to OCR with reduced training cost.

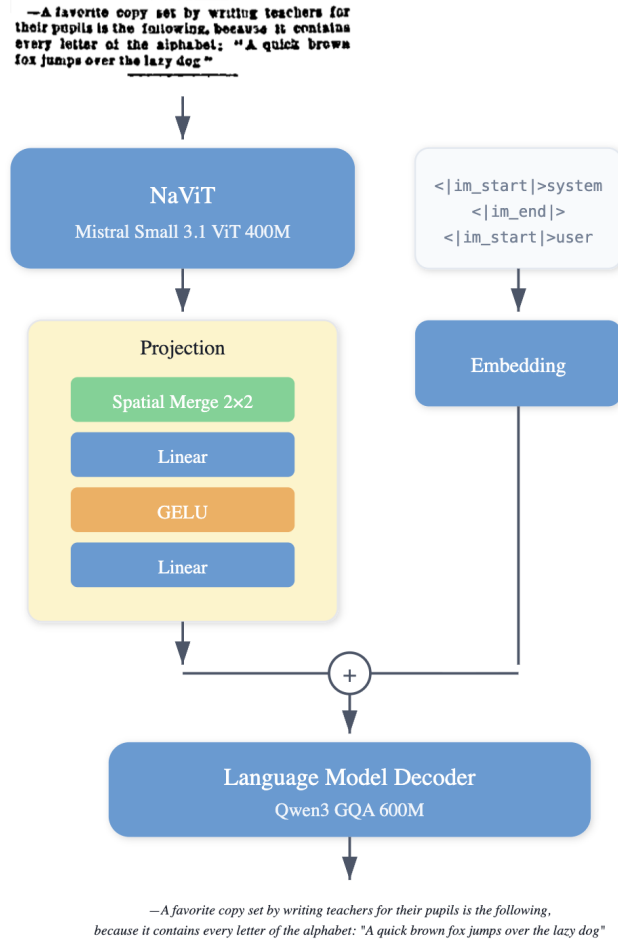


Figure 1: Model architecture.

2.2 LightOnOCR-1

The first version of LightOnOCR [13], established the core architecture described above. It was developed using supervised training on the PDF Association (PDFA) dataset [17], using transcriptions generated by Qwen2-VL-72B-Instruct [18] as teacher supervision. Training used a maximum longest-edge resolution of 1024 pixels.

2.3 LightOnOCR-2

LightOnOCR-2 keeps the same architecture but significantly updates both the data and the training recipe. We scale the pretraining mixture from 17M to 43M pages (Section 3), with stronger coverage of scanned documents, scientific PDFs, and European languages with an emphasis on French. Supervision quality is improved by leveraging a stronger teacher, Qwen3-VL-235B-A22B-Instruct [16], and by improving conversion and normalization so that targets better preserve layout and clean L^AT_EX formatting. We also increase the maximum longest-edge resolution from 1024 to 1540 pixels, improving legibility for small text and dense mathematical notation while retaining dynamic resizing for diverse page sizes. Beyond transcription, we train an image-localization variant that predicts bounding boxes for embedded images by extending the output format with normalized coordinates; to avoid OCR regressions, we introduce coordinate supervision during pretraining via a resume strategy and then refine localization with RLVR using IoU-based objectives (Section 4.2). Finally, we apply lightweight weight-space techniques, checkpoint averaging and task-arithmetic merging, to combine complementary gains across runs and to control trade-offs between OCR quality and bbox accuracy.

3 Datasets and Preprocessing

3.1 Dataset Scale and Composition

Both LightOnOCR versions are trained on large-scale document OCR corpora built primarily through distillation: a strong vision–language teacher produces naturally ordered transcriptions (Markdown with \LaTeX spans) from rendered PDF pages. Compared to LightOnOCR-1B, LightOnOCR-2-1B scales up the data mixture and improves supervision quality by upgrading the teacher model from *Qwen2-VL-72B-Instruct* [18] to *Qwen3-VL-235B-A22B-Instruct*, yielding more faithful mathematical notation and fewer formatting artifacts. The LightOnOCR-2-1B mixture combines teacher-annotated document pages from multiple permissibly usable sources, including scanned material for robustness, as well as auxiliary data to broaden layout coverage.

In addition to full pages, we include document-region crops (paragraphs, headers, abstracts, and general snippets) annotated with GPT-4o [19] to expose the model to varied formats, and we add explicit blank-page examples to enforce a consistent target for empty inputs and mitigate looping or hallucination behaviors. To better cover scientific documents, we also incorporate \TeX -derived supervision obtained by compiling raw arXiv sources with an *nvpdftex* [20] pipeline (Section 3.3), and we complement the mix with publicly available OCR datasets for additional diversity [9]. We release the PDFA-derived annotated subset under license terms that match the underlying PDFA source data as lightonai/LightOnOCR-mix-0126.

During large-scale annotation, we observed that the teacher occasionally emitted figure bounding box coordinates even when not explicitly prompted to do so. Manual inspection of a sampled subset showed these boxes to be highly accurate. To keep the base OCR objective strictly focused on transcription, we removed coordinate traces from the main supervised training targets; however, we retained them as a separate supervision signal for the bounding-box addition procedure described in Section 4.2.1. We also reformatted the coordinates to match our target output convention before training. We publicly release this extracted and normalized subset as lightonai/LightOnOCR-bbox-mix-0126.

3.2 Normalization Pipeline and data clean-up

As described above, our training corpus is assembled from heterogeneous sources (PDFA, scans, open mixtures, arXiv renders) and multiple VLM teachers, which introduces systematic but superficial inconsistencies in the raw transcriptions: stray Markdown code fences, watermark text, variable image placeholders, templated “this page is empty” messages, and occasional format drift (e.g., \LaTeX environments or HTML fragments where Markdown is expected). While these artifacts rarely affect human readability, they significantly increase target entropy and hurt both deduplication and learning stability. We therefore apply a unified normalization pipeline that maps all sources to a single, canonical target format before mixing and training.

Concretely, normalization is implemented as a sequence of lightweight, mostly deterministic transforms applied prior to hashing and filtering. We (i) sanitize the text (e.g., remove spurious Markdown ticks/code blocks and harmonize whitespace), and apply source-specific cleanup when needed. Notably, we remove recurring watermark artifacts during preprocessing so they do not pollute the deduplication procedure. (ii) homogenize special cases such as full-page embedded images and blank pages by mapping them to fixed targets (respectively a single standard image placeholder and the empty string), and (iii) perform loop and repetition filtering and deduplication on the normalized text. To retain control over the proportion of degenerate-but-common cases, we also separate dedicated pools of empty pages, which were then re-injected at a chosen rate during training as mentioned in Section 3.1.

Finally, we run a \LaTeX conversion and validation pass to enforce formatting invariants across the full mixture: \LaTeX commands are restricted to math spans, headers and sections are converted to markdown, tables are standardized (we use HTML targets to reduce ambiguity), and math expressions are checked for KaTeX [21] compatibility. The conversion step emits structured metadata (success/partial/timeout, unresolved references, missing figure numbering, KaTeX compatibility), enabling simple, reproducible filtering rules when constructing the final training mixture.

3.3 *nvpdftex* data curation pipeline

High-quality OCR supervision requires pairing rendered page images with faithful, layout-consistent transcriptions. In earlier iterations we relied on a Nougat-style PDF parsing pipeline [7], but in practice we found it difficult to obtain sufficiently reliable (image, markup) pairs at scale for training: conversion errors, reading order issues, and imperfect alignment between rendered pages and extracted markup introduce noise that can hinder learning. For LightOnOCR-2, we revamped the arXiv extraction pipeline around *nvpdftex*, a recently released NVIDIA toolchain that hooks directly into the *pdf \TeX* engine to produce pixel-aligned annotations without heuristic matching. Concretely, *nvpdftex* compiles \TeX sources and emits (i) a PNG rendering of each page, (ii) structured text targets (Markdown

or HTML) for each region, (iii) pixel-accurate bounding boxes with semantic classes (e.g. headers/footers, captions, tables, formulas, pictures), and (iv) page-level metadata (e.g. image dimensions) [20, 22]. We additionally use this pipeline to generate high-quality figure/image boxes for the arXiv subset used in our bbox RLVR experiments (Section 4.2.2); these arXiv bounding boxes are used for RL supervision rather than included in the main pretraining mixture.

3.4 LightOnOCR-bbox-bench: New Image Localization Benchmark

LightOnOCR-bbox-bench While OCR benchmarks are widely used, there are no standardized benchmarks that specifically measure how well end-to-end vision-language models *localize* images within documents. To fill this gap, we introduce **LightOnOCR-bbox-bench**, released with this work and composed of two subsets: (i) a manually reviewed subset derived from OlmOCR-Bench [8] pages (290 samples) and (ii) an automatically annotated arXiv subset generated with `nvpdf.tex` (565 samples) and filtered programmatically. We report F_1 at IoU threshold 0.5, mean IoU, and count accuracy (exact match on the number of predicted boxes), and evaluate separately on the manual OlmOCR-derived subset and the automatic arXiv+`nvpdf.tex` subset.

4 Training

4.1 Pretraining

Training setup We train on a large mixed corpus of OCR datasets described in Section 3, with filtering to remove missing references, numberless figures, KaTeX-incompatible samples, and long completions (capped at 3100 tokens). Document pages are rendered at 200 DPI during training (except for crops which were already available as images) and resized to a maximum longest edge of 1540 pixels for computational efficiency. We apply moderate document augmentations such as bitmap corruption, erosion/dilation, small affine shears, shift-scale-rotate, 90° rotations, and mild grid distortions, so that a page receives at least one augmentation with probability 0.22 (and we use a more aggressive regime for blank-page examples). We optimize a next-token prediction objective but mask part of the loss: the loss is computed only on assistant tokens, excluding prompt tokens (system prompt and special tokens) as well as image tokens. Optimization uses AdamW with no weight decay, a peak learning rate of 10^{-4} , a cosine learning rate schedule with a 100-step warmup, a global batch size of 384 samples, and a maximum sequence length of 6144 tokens. Training is distributed with DDP over 96 NVIDIA H100 GPUs (80 GB) using bf16 precision and FlashAttention-2 [23].

4.2 Reinforcement Learning with Verifiable Rewards

We apply RLVR [14], where rewards are computed by automatic checks that can be evaluated deterministically on model outputs (e.g., binary unit tests on synthetic documents). This allows us to directly optimize for specific OCR failure modes without having to annotate extra data.

Training setup We start from the pretraining checkpoints (LightOnOCR-2-1B-base for OCR and LightOnOCR-2-1B-bbox-base for localization) and train with GRPO [24] for one epoch with AdamW at learning rate 4×10^{-5} and KL regularization strength $\beta = 0.01$. We use group-scaled rewards with token-level importance sampling and sample multiple rollouts per prompt (28 for OCR and 14 for bbox). Training is implemented with the Hugging Face TRL library [25], and rollouts are generated with vLLM for increased efficiency.

We apply two RLVR recipes: an OCR-focused variant that extends OlmOCR unit tests with additional rewards, and a bbox-focused variant that optimizes IoU-based localization rewards.

4.2.1 OlmOCR-2 Style RLVR Recipe

We build on the OlmOCR-2 RLVR recipe [9], where rewards are derived from synthetic OlmOCR-Bench-style unit tests, and extend it with additional checks tailored to scientific documents. In addition to scoring completions by the fraction of tests they pass, we (i) penalize low-entropy repetition loops using a compression-based heuristic and ensuring proper EOS termination, (ii) reward mathematical correctness by extracting math spans and verifying they render successfully with KaTeX, (iii) enforce clean math formatting by rejecting common artifacts such as HTML tags, misused Markdown italics for variables, and unbalanced \LaTeX delimiters or environments, and (iv) remove the frontmatter reward that encourages the model to output document metadata at the top of its response. Finally, for the headers/footers category, we change the *absence* reward to instead reward *presence* of headers, footers, and page numbers, encouraging high-fidelity extraction of all visible content.

4.2.2 Bounding Box RLVR Recipe

To complement OCR with image localization, we extend the output format for embedded images to `![image](image_N.png)x1,y1,x2,y2`, where coordinates are normalized to $[0, 1000]$. Throughout pretraining, the model is already trained to emit the image placeholder `![image](image_N.png)` whenever an image is present; bounding box learning therefore mainly adds *where* the image is, not *whether* it exists. We enable this capability by resuming pretraining from the base checkpoint and continuing on a mixture stage that includes bbox-annotated pages, providing a cold start for RL. This pretraining integration preserves OCR performance, enabling joint OCR and image localization.

We then further improve image localization with RLVR using an IoU-based reward. The full reward definition is given in Appendix D.

4.2.3 Model Averaging and Merging

We use **checkpoint averaging** by souping the last 5 checkpoints, which consistently outperforms any single checkpoint. This yields our strong supervised pretraining baseline `LightOnOCR-2-1B-base`. We then apply **RLVR** on top of this base to obtain our best OCR model `LightOnOCR-2-1B`. In parallel, we train a bbox-capable variant by resuming supervised pretraining with coordinate annotations introduced during training, producing `LightOnOCR-2-1B-bbox-base`, and further refine it with bbox-focused RLVR to obtain `LightOnOCR-2-1B-bbox`. Finally, we apply **task arithmetic** merging, $\theta_{\text{merge}} = \theta_{\text{base}} + \alpha(\theta_{\text{rl}} - \theta_{\text{base}})$, to form `LightOnOCR-2-1B-ocr-soup` by merging `LightOnOCR-2-1B` into the averaged base with $\alpha = 0.4$. We then construct `LightOnOCR-2-1B-bbox-soup` by merging `LightOnOCR-2-1B-ocr-soup` into the bbox-specialized checkpoint `LightOnOCR-2-1B-bbox` (used as the base) with $\alpha = 0.1$, yielding an explicit OCR–bbox trade-off without additional training. Our training targets retain headers/footers, and in RLVR we flip OlmOCR’s header/footer *absence* tests to reward *presence* of this text. We also applied the OCR RLVR recipe to `LightOnOCR-1B-1025` to obtain `LightOnOCR-1B-1025-GRPO` for reference.

5 Results

We evaluate `LightOnOCR-2-1B` on OlmOCR-Bench [8] as our primary OCR benchmark. We additionally report OmniDocBench v1.0 [26] results in Appendix C.2. For localization, we evaluate on `LightOnOCR-bbox-bench` (Section 3.4). Unless otherwise stated, we use a single-pass evaluation without test-time heuristics (e.g., rotation sweeps or retries); inference details for `LightOnOCR` models are provided in Appendix B.

5.1 OlmOCR-Bench

We report OlmOCR-Bench results without the *headers/footers* category as originally defined, since it rewards *omitting* visible content (e.g., titles and page numbers) whereas our objective is full-page transcription; systems that explicitly suppress these regions can score well without improving full-page extraction quality, and even empty outputs can achieve a perfect score. We evaluate all models without test-time heuristics (e.g., retries or rotation correction) to reflect raw model behavior.

Table 1 shows that `LightOnOCR-2-1B` achieves the highest overall score (83.2 ± 0.9) among evaluated systems, outperforming substantially larger end-to-end models while using only 1B parameters and being end-to-end trainable. Improvements are broad across categories, with particularly strong scores on ArXiv, old scans math, and table-heavy documents, highlighting the benefit of higher-quality data, increased scientific coverage, and higher-resolution training.

Comparing `LightOnOCR-2-1B-base` to `LightOnOCR-2-1B` isolates the effect of RLVR, which improves overall performance and reduces common generation failures such as repetition loops (Appendix C.4). Introducing bbox prediction (`LightOnOCR-2-1B-bbox`) yields a small OCR quality drop relative to the base checkpoint while enabling localization; task-arithmetic merging partially recover OCR performance and provide an explicit OCR–bbox trade-off (`bbox-soup`). As we optimize for the presence of headers/footers, under the original OlmOCR-Bench definition (rewarding suppression), our `headers_footers` score decreases; see Appendix C.1 for details. When applying the same recipe to our previous model, we observe similar gains on OCR performance, see `LightOnOCR-1B-1025-GRPO` in Table 1.

5.2 Image Bounding Box Detection

Table 2 reports bounding-box detection on `LightOnOCR-bbox-bench`. The goal is to measure whether a compact end-to-end OCR model can localize embedded images while retaining strong transcription quality. We compare against

Model	End-to-end	Size (B)	ArXiv	Old Scans	Math Tables	Old Scans	Multi-column	Long Tiny Text	Base	Overall
Mistral OCR 3 API	-	-	85.6	69.7	85.5	43.5	81.2	88.5	99.7	79.1 \pm 1.0
Gemini Flash 2	-	-	32.1	56.3	61.4	27.8	58.7	84.4	94.0	59.2 \pm 1.1
Qwen2.5-VL-8B	✓	8	63.1	65.7	67.3	38.6	68.3	49.1	98.3	64.3 \pm 1.2
olmOCR v0.3.0	✗	8	78.6	79.9	72.9	43.9	77.3	81.2	98.9	76.1 \pm 1.1
MonkeyOCR-pro-3B	✗	3	83.8	68.8	74.7	36.1	76.6	80.1	95.3	73.6 \pm 1.0
dots.ocr	✗	3	82.1	64.2	88.3	40.9	82.4	81.2	99.5	76.9 \pm 1.0
DeepSeekOCR	✓	3	77.5	74.5	77.3	33.1	67.3	83.0	99.3	73.1 \pm 1.0
Chandra-9B	✓	9	82.2	80.3	88.0	50.4	81.2	92.3	99.9	81.7 \pm 0.9
olmOCR-2-8B	✓	8	82.9	82.1	84.3	48.3	84.3	81.4	99.7	80.4 \pm 1.1
MonkeyOCR-pro-1.2B	✗	1.2	80.5	62.9	71.1	32.9	68.3	74.0	92.6	68.9 \pm 1.1
MinerU2.5	✗	1.2	76.6	54.6	84.9	33.7	78.2	81.2	83.5	70.4 \pm 1.0
PaddleOCR-VL	✗	0.9	85.7	71.0	84.1	37.8	79.9	85.7	98.5	77.5 \pm 1.0
LightOnOCR-1B-1025	✓	1	81.4	71.6	76.4	35.2	80.0	88.7	99.5	76.1 \pm 1.1
LightOnOCR-1B-1025-GRPO	✓	1	86.5	73.8	74.5	32.9	85.1	91.6	99.7	77.7 \pm 1.0
LightOnOCR-2-1B-base	✓	1	84.9	80.3	86.7	47.0	84.6	89.1	99.8	81.8 \pm 0.9
LightOnOCR-2-1B-bbox-base	✓	1	84.6	78.6	84.7	46.0	83.8	88.0	99.8	80.8 \pm 0.9
LightOnOCR-2-1B-bbox	✓	1	86.9	74.7	88.6	39.7	85.0	86.4	99.8	80.2 \pm 0.9
LightOnOCR-2-1B-bbox-soup	✓	1	86.1	77.9	88.2	41.2	85.4	87.3	99.7	80.8 \pm 0.9
LightOnOCR-2-1B-ocr-soup	✓	1	86.8	81.2	89.0	45.4	84.2	90.3	99.7	82.4 \pm 0.9
LightOnOCR-2-1B	✓	1	89.6	85.6	89.0	42.2	84.8	91.4	99.6	83.2 \pm 0.9

Table 1: OlmOCR-Bench results (headers/footers category excluded; see Appendix C.1). Per-column best is highlighted in blue and second best in bold. Results are taken from the corresponding published works; we additionally evaluate DeepSeekOCR and the Mistral OCR 3 API since they do not report OlmOCR-Bench numbers. Inference details for our models are provided in Appendix B.

Chandra-9B [12] under the same evaluation protocol and restrict evaluation to visual elements (figures/images), ignoring other layout categories.

Table 2: Bounding box detection on LightOnOCR-bbox-bench.

Model	OlmOCR (290)			arXiv (565)		
	F_1 @0.5	IoU	Count Acc.	F_1 @0.5	IoU	Count Acc.
Chandra-9B	0.75	0.71	75.2	0.81	0.77	81.8
LightOnOCR-2-1B-bbox	0.78	0.70	83.8	0.83	0.77	85.0
LightOnOCR-2-1B-bbox-soup	0.76	0.67	80.7	0.82	0.76	85.1

Localization quality LightOnOCR-2-1B-bbox improves F_1 @0.5 and count accuracy over the 9B baseline on both subsets, while achieving comparable mean IoU. This indicates reliable detection of both the presence and number of figures, with accurate localization, despite the substantially smaller model size.

5.3 Efficiency

Beyond accuracy, we measure throughput to characterize the practical speed-quality trade-off of end-to-end OCR models. We measure inference efficiency by running the full OlmOCR-Bench evaluation (1,403 pages) end-to-end and reporting pages/sec as the total number of pages divided by the wall-clock time to complete the benchmark. We prefer pages/sec over tokens/sec, since tokenization and output lengths differ across models and formats, making tokens/sec less comparable. Each model was run using its official library and the inference parameters recommended by its respective authors to ensure a fair comparison. Table 3 compares LightOnOCR-2-1B against the main end-to-end baselines; a full comparison with additional systems is provided in Appendix C.3.

Model	Dtype	Size (B)	Throughput (pages/sec)
LightOnOCR-2	BF16	1	5.71
olmOCR-2	FP8	8	3.28
Chandra	BF16	9	1.70

Table 3: Inference throughput on a single NVIDIA H100 (80 GB).

These results show that LightOnOCR-2 provides substantially higher throughput than larger end-to-end baselines, making it practical for high-volume document processing.

6 Scope and Limitations

LightOnOCR-2-1B models are designed for printed document understanding and perform particularly well on: (i) scientific PDFs, including dense typography and accurate \LaTeX math transcription (e.g., strong arXiv and “old scans math” results in Table 1); (ii) scans of typed documents, including moderately degraded, noisy or rotated scans; (iii) European languages and Latin scripts, reflecting the distributional emphasis of the pretraining mixture; and (iv) layout-heavy pages such as multi-column documents and long-form tables, where faithful reading order and structure are critical.

Despite strong overall robustness, we note two important limitations. First, multilingual performance outside of European / Latin-script languages is not fully supported: our training mix and normalization pipeline prioritize Latin-script documents, and some non-Latin scripts (e.g., CJK or Arabic) can exhibit degraded fidelity or inefficient tokenization compared to the in-scope languages (as shown in Appendix A it is as expected all the more evident for pruned models). Second, handwritten text transcription remains inconsistent: while LightOnOCR-2-1B benefits from scan coverage, its supervision is primarily derived from printed or typeset sources, and cursive or unconstrained handwriting is not a target use-case for the released checkpoints. We view these as promising directions for future work through targeted data collection and evaluation.

7 Conclusion

We introduce LightOnOCR-2-1B a 1B-parameter end-to-end OCR VLM setting new state-of-the-art on OlmoOCR-Bench. Building on top of the LightOnOCR architecture, setup and insight, we detailed the key factors behind its improved performance: a substantially larger and cleaner pretraining mixture, stronger document normalization and conversion pipelines, and higher-resolution training with targeted augmentations. We further presented an image-localization variant trained to predict bounding boxes without degrading OCR by introducing coordinates during pretraining and refining them with RLVR. Finally, we showed that lightweight weight-space techniques, checkpoint averaging and task-arithmetic merging, provide practical gains and enable explicit control of the OCR-bbox trade-off. We release model weights, datasets, and the LightOnOCR-bbox-bench benchmark to support reproducible research on high-fidelity document extraction and localization.

Acknowledgments

This work was granted access to the HPC resources of IDRIS under GENCI allocations AS011016449, A0181016214, and A0171015706, enabling us to use the Jean Zay supercomputer. All RL experiments were run on our in-house H200 nodes. We thank Stéphane Réquena and the IDRIS support team for their valuable help. We also thank the LightOn team for their support in making this release possible, with special thanks to Antoine Chaffin and Amélie Chatelain for their help throughout the release process.

References

- [1] Ray Smith. An overview of the tesseract ocr engine. In *Proceedings of the International Conference on Document Analysis and Recognition (ICDAR)*, 2007.
- [2] Baoguang Shi, Xiang Bai, and Cong Yao. An end-to-end trainable neural network for image-based sequence recognition and its application to scene text recognition. *arXiv preprint arXiv:1507.05717*, 2015.
- [3] Minghao Li, Tengchao Lv, Jingye Chen, Lei Cui, Yijuan Lu, Dinei Florencio, Cha Zhang, Zhoujun Li, and Furu Wei. Trocr: Transformer-based optical character recognition with pre-trained models. *arXiv preprint arXiv:2109.10282*, 2021.
- [4] PaddlePaddle. Paddleocr, 2025. Accessed 2026-01-17.
- [5] Yuning Du, Chenxia Li, Ruoyu Guo, Xiaoting Yin, Weiwei Liu, Jun Zhou, Yifan Bai, Zilin Yu, Yehua Yang, Qingqing Dang, and Haoshuang Wang. Pp-ocr: A practical ultra lightweight ocr system. *arXiv preprint arXiv:2009.09941*, 2020.
- [6] anonymous or see arXiv page. Mineru: An open-source solution for precise document content extraction. *arXiv preprint arXiv:2409.18839*, 2024.

[7] Lukas Blecher, Guillem Cucurull, Thomas Scialom, and Robert Stojnic. Nougat: Neural optical understanding for academic documents. In *International Conference on Learning Representations*, 2024.

[8] Jake Poznanski, Aman Rangapur, Jon Borchardt, Jason Dunkelberger, Regan Huff, Daniel Lin, Christopher Wilhelm, Kyle Lo, and Luca Soldaini. olmocr: Unlocking trillions of tokens in pdfs with vision language models. *arXiv preprint arXiv:2502.18443*, 2025.

[9] Jake Poznanski, Luca Soldaini, and Kyle Lo. olmocr 2: Unit test rewards for document ocr. 2025.

[10] Yumeng Li, Guang Yang, Hao Liu, Bowen Wang, and Colin Zhang. dots.ocr: Multilingual document layout parsing in a single vision-language model. *arXiv preprint arXiv:2512.02498*, 2025.

[11] Cheng Cui, Ting Sun, Suyin Liang, Tingquan Gao, Zelun Zhang, Jiaxuan Liu, Xueqing Wang, Changda Zhou, Hongen Liu, Manhui Lin, Yue Zhang, Yubo Zhang, Handong Zheng, Jing Zhang, Jun Zhang, Yi Liu, Dianhai Yu, and Yanjun Ma. Paddleocr-vl: Boosting multilingual document parsing via a 0.9b ultra-compact vision-language model. *arXiv preprint arXiv:2510.14528*, 2025.

[12] Datalab. Chandra: Ocr model that handles complex tables, forms, handwriting with full layout. <https://github.com/datalab-to/chandra>, 2025. GitHub repository, accessed 2026-01-16.

[13] Said Taghadouini, Baptiste Aubertin, and Adrien Cavaillès. Lightonocr-1b: Making knowledge machine-readable. <https://www.lighton.ai/lighton-blogs/making-knowledge-machine-readable>, 2025. LightOnOCR v1 blog post.

[14] Nathan Lambert, Jacob Daniel Morrison, Valentina Pyatkin, Shengyi Huang, Hamish Ivison, Faeze Brahman, Lester James Validad Miranda, Alisa Liu, Nouha Dziri, Xinxin Lyu, Yuling Gu, Saumya Malik, Victoria Graf, Jena D. Hwang, Jiangjiang Yang, Ronan Le Bras, Oyvind Tafjord, Christopher Wilhelm, Luca Soldaini, Noah A. Smith, Yizhong Wang, Pradeep Dasigi, and Hanna Hajishirzi. Tülu 3: Pushing frontiers in open language model post-training. *ArXiv*, abs/2411.15124, 2024.

[15] Mistral AI. Mistral small 3.1. <https://mistral.ai/news/mistral-small-3-1/>, 2025.

[16] Qwen Team. Qwen3 technical report, 2025.

[17] Pixparse. Pdf association dataset. <https://huggingface.co/datasets/pixparse/pdfa-eng-wds>, 2025. Hugging Face Datasets.

[18] Peng Wang, Shuai Bai, Sinan Tan, Shijie Wang, Zhihao Fan, Jinze Bai, Keqin Chen, Xuejing Liu, Jialin Wang, Wenbin Ge, Yang Fan, Kai Dang, Mengfei Du, Xuancheng Ren, Rui Men, Dayiheng Liu, Chang Zhou, Jingren Zhou, and Junyang Lin. Qwen2-vl: Enhancing vision-language model’s perception of the world at any resolution. *arXiv preprint arXiv:2409.12191*, 2024.

[19] OpenAI. Gpt-4o system card. <https://cdn.openai.com/gpt-4o-system-card.pdf>, August 2024. Accessed: 2026-01-14.

[20] NVIDIA. nvtexlive: Fork of tex live with hooks to generate ocr annotations (nvpdfex toolchain). <https://github.com/NVIDIA/nvtexlive>, 2025.

[21] KaTeX Contributors. KaTeX: Fast math typesetting for the web. <https://katex.org/>, 2025. Version 0.16.27.

[22] Ilia Karmanov et al. éclair: Extracting content and layout with integrated reading order for documents. 2025.

[23] Tri Dao. Flashattention-2: Faster attention with better parallelism and work partitioning, 2023.

[24] Zhihong Shao, Peiyi Wang, Qihao Zhu, Runxin Xu, Junxiao Song, Mingchuan Zhang, et al. Deepseekmath: Pushing the limits of mathematical reasoning in open language models. *arXiv preprint arXiv:2402.03300*, 2024.

[25] Hugging Face. TRL: Transformer reinforcement learning, 2026. Accessed: 2026-01-18.

[26] Linke Ouyang, Yuan Qu, Hongbin Zhou, Jiawei Zhu, Rui Zhang, Qunshu Lin, Bin Wang, Zhiyuan Zhao, Man Jiang, Xiaomeng Zhao, Jin Shi, Fan Wu, Pei Chu, Minghao Liu, Zhenxiang Li, Chao Xu, Bo Zhang, Botian Shi, Zhongying Tu, and Conghui He. Omnidocbench: Benchmarking diverse pdf document parsing with comprehensive annotations, 2024.

[27] Gabriel Ilharco, Marco Túlio Ribeiro, Mitchell Wortsman, Suchin Gururangan, Ludwig Schmidt, Hannaneh Hajishirzi, and Ali Farhadi. Editing models with task arithmetic. In *International Conference on Learning Representations (ICLR)*, 2023.

A Vocabulary Pruning

The Qwen3 decoder uses a 151,936-token multilingual vocabulary, much of which is unused for language-specific OCR. We investigate frequency-based vocabulary pruning for English/French documents, reducing to 51k, 32k, and 16k tokens while preserving tokenizer integrity through recursive sub-token frequency propagation.

Table 4 summarizes the trade-offs. Pruning to 16k tokens reduces parameters by 13.8% with minimal OCR degradation on English benchmarks (75.4% vs 76.1% on OlmOCR-Bench). The 32k variant achieves the best speed-accuracy balance: 11.6% faster inference while retaining 96% of base performance. However, non-Latin scripts (Arabic, Chinese) experience $\sim 3\times$ token count inflation as script-specific tokens are removed. These experiments were conducted on LightOnOCR-1; we release the pruned variants as LightOnOCR-0.9B-32k-1025¹ and LightOnOCR-0.9B-16k-1025².

Vocab	Params (M)	OlmOCR Overall	Speedup vs Base	Tokens/page (EN/ZH)
151k (Base)	1005.6	76.1	—	475 / 950
51k	902.5	67.7	+9.5%	485 / 2220
32k	883.6	73.1	+11.6%	510 / 2750
16k	866.8	75.4	+3.9%	575 / 3200

Table 4: Vocabulary pruning trade-offs. Smaller vocabularies reduce parameters and improve speed for Latin-script languages but degrade tokenization for Chinese (ZH) and other non-Latin scripts.

B Inference Details

LightOnOCR models are evaluated with $T = 0.2$, $\text{top_}p = 0.9$ and $\text{top_}k = 0$. For OlmOCR-Bench, we use three independent generations(3 repeats) per page; maximum resolution set to 1540, no test-time heuristics (retries/rotations) are used.

C Additional Results

C.1 OlmOCR Headers/Footers

OlmOCR-Bench includes a `headers_footers` category whose unit tests reward *absence* of header and footer text. In contrast, our training objective is full-page transcription: throughout both pretraining and RLVR, our targets retain all visible content, including page numbers, running headers, titles, and footers. Moreover, in RLVR we explicitly flip the header/footer *absence* tests to reward *presence* of header and footer text. As a result, when evaluated under the *original* OlmOCR-Bench scoring, models optimized for full-page extraction can obtain lower `headers_footers` scores. Table 5 reports this metric for all released checkpoints.

Checkpoint	OlmOCR headers_footers score
LightOnOCR-2-1B	19.74
LightOnOCR-2-1B-base	31.05
LightOnOCR-2-1B-bbox	29.34
LightOnOCR-2-1B-bbox-base	31.05
LightOnOCR-2-1B-bbox-soup	29.47
LightOnOCR-2-1B-ocr-soup	25.13

Table 5: OlmOCR-Bench `headers_footers` scores under the *original* benchmark definition (rewarding absence of header/footer text). Our models are trained for full-page transcription, so this metric is not aligned with our objective.

C.2 OmniDocBench Results

We report results on OmniDocBench v1.0 [26] in Table 6. Its language-split reporting provides a complementary view—most notably for reading order and structured layout fidelity. However, OmniDocBench relies heavily on

¹<https://huggingface.co/lightonai/LightOnOCR-0.9B-32k-1025>

²<https://huggingface.co/lightonai/LightOnOCR-0.9B-16k-1025>

edit-distance-based metrics that are sensitive to formatting conventions, and the benchmark primarily targets English and Chinese documents. We therefore treat it as a secondary evaluation signal.

Model	Size (B)	Overall ^{Edit ↓}		Text ^{Edit ↓}		Formula ^{Edit ↓}		Formula ^{CDM ↑}		Table ^{TEDS ↑}		Table ^{Edit ↓}		Read Order ^{Edit ↓}	
		EN	ZH	EN	ZH	EN	ZH	EN	ZH	EN	ZH	EN	ZH	EN	ZH
Gemini2.0-flash	-	0.191	0.264	0.091	0.139	0.389	0.584	77.6	43.6	79.7	78.9	0.193	0.206	0.092	0.128
Qwen2-VL-72B	72	0.252	0.327	0.096	0.218	0.404	0.487	82.2	61.2	76.8	76.4	0.387	0.408	0.119	0.193
MonkeyOCR-pro-3B	3	0.138	0.206	0.067	0.107	0.246	0.421			81.5	87.5	0.139	0.111	0.100	0.185
dots.ocr	3	0.125	0.160	0.032	0.066	0.329	0.416			88.6	89.0	0.099	0.092	0.040	0.067
DeepSeek-OCR (Gundam-M)	3	0.123	0.157	0.049	0.087	0.242	0.377					0.147	0.08	0.056	0.085
MonkeyOCR-pro-1.2B	1.2	0.146	0.221	0.068	0.118	0.272	0.452	76.663	63.282	81.342	85.504	0.149	0.134	0.093	0.179
MinerU2.5	1.2	0.111	0.174	0.050	0.074	0.258	0.473			88.3	89.2	0.089	0.083	0.045	0.068
PaddleOCR-VL	0.9	0.105	0.126	0.041	0.062	0.241	0.316			88.0	92.1	0.093	0.062	0.045	0.063
LightOnOCR-1B-1025	1	0.234	0.392	0.090	0.380	0.486	0.621			70.1	63.7	0.262	0.307	0.098	0.259
LightOnOCR-1B-1025-GRPO	1	0.254	0.390	0.267	0.463	0.384	0.586			65.3	59.6	0.305	0.316	0.061	0.195
LightOnOCR-2-1B	1	0.146	0.263	0.082	0.317	0.339	0.438			85.7	82.7	0.112	0.132	0.050	0.167
LightOnOCR-2-1B-bbox	1	0.152	0.305	0.080	0.343	0.316	0.523			82.1	78.0	0.144	0.171	0.068	0.181
LightOnOCR-2-1B-base	1	0.150	0.281	0.059	0.289	0.340	0.530			82.9	80.5	0.140	0.144	0.060	0.161
LightOnOCR-2-1B-bbox-base	1	0.153	0.277	0.062	0.303	0.341	0.489			82.0	80.9	0.146	0.145	0.064	0.173
LightOnOCR-2-1B-ocr-soup	1	0.150	0.255	0.071	0.295	0.338	0.437			84.3	83.1	0.126	0.124	0.066	0.164

Table 6: OmniDocBench v1.0 (EN/ZH) results. Per-column best within each size group is highlighted in blue. LightOnOCR-2 shows a clear improvement over LightOnOCR-1, with LightOnOCR-2-1B ranking among the strongest models in its size class.

C.3 Extended Efficiency Comparison

Table 7 extends the efficiency comparison from Section 5.3 to include additional OCR systems. Each model was run using its official library and the inference parameters recommended by its respective authors. We prefer pages/sec over tokens/sec since tokenization and output lengths differ across models, making tokens/sec less comparable.

Model	Dtype	Size (B)	Throughput (pages/sec)	Speedup vs slowest
LightOnOCR-2	BF16	1	5.71	6.49×
olmOCR-2	FP8	8	3.28	3.73×
olmOCR-2	BF16	8	2.54	2.89×
DeepSeek-OCR	BF16	3	2.36	2.68×
PaddleOCR-VL	BF16	1	2.14	2.43×
Chandra	BF16	9	1.70	1.93×
dots.ocr	BF16	3	0.88	1.00×

Table 7: Full inference throughput comparison on a single NVIDIA H100 (80 GB).

C.4 RLVR Effect on Repetition Loops

To quantify repetition loops, we scan OlmOCR-Bench generations with a low-entropy detector based on the ZLIB compression ratio (flagging outputs with ratio < 0.13). Table 8 summarizes the fraction of flagged generations, showing a reduction after RLVR, consistent with our repetition-focused reward component (Section 4.2).

Checkpoint	% Loopy
LightOnOCR-2-1B-base	1.14%
LightOnOCR-2-1B	0.50%

Table 8: Loopy generations on OlmOCR-Bench.

D Bounding Box RLVR Reward

Let I_{gt} and I_{pred} denote the sets of image IDs present in the ground-truth and predicted outputs for a page, and let \mathcal{B}_i^{gt} and \mathcal{B}_i^{pred} be the corresponding boxes for image ID i . We compute the mean IoU over matched IDs and scale it by an

ID-overlap factor:

$$R_{\text{bbox}} = \left(\frac{1}{|I_{\cap}|} \sum_{i \in I_{\cap}} \text{IoU}(\mathcal{B}_i^{\text{pred}}, \mathcal{B}_i^{\text{gt}}) \right) \cdot \frac{|I_{\cap}|}{\max(|I_{\text{gt}}|, |I_{\text{pred}}|)}, \quad I_{\cap} = I_{\text{gt}} \cap I_{\text{pred}}. \quad (1)$$

This formulation rewards accurate localization for correctly predicted image IDs while penalizing missing and hallucinated boxes through the overlap factor.

D.1 Task-Arithmetic Model Merging

Because OCR quality and localization accuracy can pull model behavior in different directions, we use weight-space merging to expose a controllable trade-off between the two directions. We apply task-arithmetic merging [27] to combine an OCR-specialized checkpoint with a bounding-box (bbox) specialized checkpoint while explicitly controlling their trade-off. Concretely, we interpolate in weight space as $\theta = \theta_{\text{bbox}} + \alpha(\theta_{\text{ocr}} - \theta_{\text{bbox}})$ with $\alpha \in [0, 1]$, and evaluate the resulting models on both OCR and bbox localization metrics (Figure 2). The difference vector $(\theta_{\text{ocr}} - \theta_{\text{bbox}})$ can be interpreted as an OCR “task vector” added to the bbox model with strength α , yielding a single merged checkpoint with no additional training cost and unchanged inference. As expected, OCR performance increases with α , but bbox detection degrades beyond $\alpha > 0.4$ and collapses for $\alpha \geq 0.6$, suggesting that localization-specific parameters are progressively overwritten. In our experiments, the best balance occurs around $\alpha \approx 0.1$, which preserves strong bbox quality (IoU= 0.677) while improving OCR performance to 80.88%.

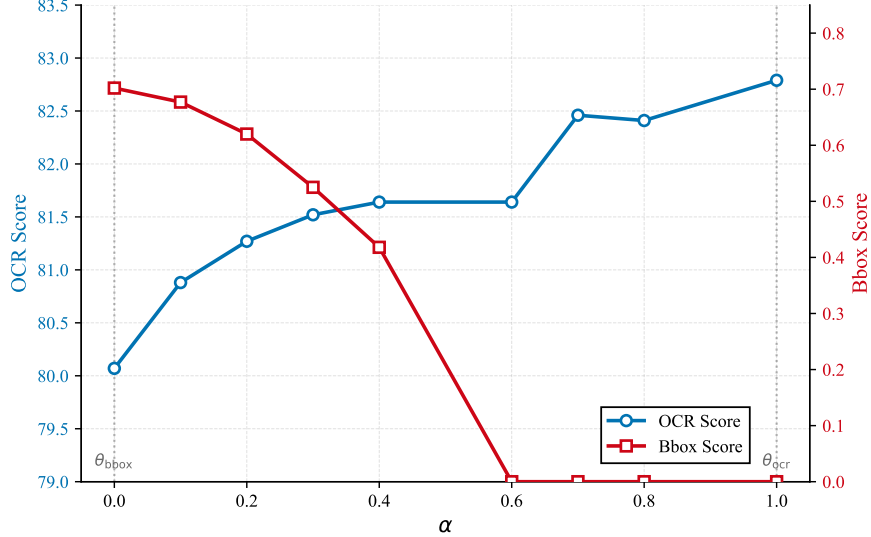


Figure 2: Task-arithmetic interpolation between a bbox-specialized and an OCR-specialized checkpoint.

E Examples

We provide here some examples of transcriptions highlighting the capabilities of the OCR model family.

Client Franchises Built Over the Long Term

	2005	2014	2023	2024
Average deposits (\$B) ¹	\$887 ¹	\$487 ¹	\$1327 ¹	\$1064 ¹
Deposits market share ¹	4.5% ¹	7.9% ¹	11.4% ¹	11.3% ¹
# of top 50 markets where we are present ¹	6 (2) ¹	7 (2) ¹	22 (25) ¹	M (25) ¹
Business Banking primary market share ¹	4.0% ¹	7.2% ¹	9.5% ¹	9.7% ¹
Client investment assets (\$B) ¹	NA ¹	\$89 ¹	\$904 ¹	\$1,024 ¹
Total payments volume (\$T) ¹	NA ¹	\$16 ¹	\$59 ¹	\$65 ¹
% of digital non-card payments ¹	<20% ¹	49% ¹	79% ¹	81% ¹
Debt card sales (\$B)	NA ¹	\$40 ¹	\$194 ¹	\$204 ¹
Debt card sales (\$B)	NA ¹	\$241 ¹	\$551 ¹	\$546 ¹
Debt card sales volume (\$B) ¹	NA ¹	\$707 ¹	\$1,800 ¹	\$1,800 ¹
Credit card sales (\$B) ¹	NA ¹	\$28 ¹	\$220 ¹	\$220 ¹
Credit card loans (\$B, EOP) ¹	\$142 ¹	\$131 ¹	\$211 ¹	\$233 ¹
Credit card loans market share ¹	19% ¹	17% ¹	17% ¹	17% ¹
Active credit card customers (M) ¹	NA ¹	561 ¹	571 ¹	571 ¹
# of branches ¹	2644 ¹	5,602 ¹	4,897 ¹	4,956 ¹
# of advisors ¹	NM ¹	3,900 ¹	5,456 ¹	5,755 ¹

Client Franchises Built Over the Long Term

	2005	2014	2023	2024
Average deposits (\$B) ¹	\$887 ¹	\$487 ¹	\$1327 ¹	\$1064 ¹
Deposits market share ¹	4.5% ¹	7.9% ¹	11.4% ¹	11.3% ¹
# of top 50 markets where we are present ¹	6 (2) ¹	7 (2) ¹	22 (25) ¹	M (25) ¹
Business Banking primary market share ¹	4.0% ¹	7.2% ¹	9.5% ¹	9.7% ¹
Client investment assets (\$B) ¹	NA ¹	\$89 ¹	\$904 ¹	\$1,024 ¹
Total payments volume (\$T) ¹	NA ¹	\$16 ¹	\$59 ¹	\$65 ¹
% of digital non-card payments ¹	<20% ¹	49% ¹	79% ¹	81% ¹
Debt card sales (\$B)	NA ¹	\$40 ¹	\$194 ¹	\$204 ¹
Debt card sales (\$B)	NA ¹	\$241 ¹	\$551 ¹	\$546 ¹
Debt card sales volume (\$B) ¹	NA ¹	\$707 ¹	\$1,800 ¹	\$1,800 ¹
Credit card sales (\$B) ¹	NA ¹	\$28 ¹	\$220 ¹	\$220 ¹
Credit card loans (\$B, EOP) ¹	\$142 ¹	\$131 ¹	\$211 ¹	\$233 ¹
Credit card loans market share ¹	19% ¹	17% ¹	17% ¹	17% ¹
Active credit card customers (M) ¹	NA ¹	561 ¹	571 ¹	571 ¹
# of branches ¹	2644 ¹	5,602 ¹	4,897 ¹	4,956 ¹
# of advisors ¹	NM ¹	3,900 ¹	5,456 ¹	5,755 ¹

Consumer & Community Banking

	2005	2014	2023	2024
Average deposits (\$B) ¹	\$887 ¹	\$487 ¹	\$1327 ¹	\$1064 ¹
Deposits market share ¹	4.5% ¹	7.9% ¹	11.4% ¹	11.3% ¹
# of top 50 markets where we are present ¹	6 (2) ¹	7 (2) ¹	22 (25) ¹	M (25) ¹
Business Banking primary market share ¹	4.0% ¹	7.2% ¹	9.5% ¹	9.7% ¹
Client investment assets (\$B) ¹	NA ¹	\$89 ¹	\$904 ¹	\$1,024 ¹
Total payments volume (\$T) ¹	NA ¹	\$16 ¹	\$59 ¹	\$65 ¹
% of digital non-card payments ¹	<20% ¹	49% ¹	79% ¹	81% ¹
Debt card sales (\$B)	NA ¹	\$40 ¹	\$194 ¹	\$204 ¹
Debt card sales (\$B)	NA ¹	\$241 ¹	\$551 ¹	\$546 ¹
Debt card sales volume (\$B) ¹	NA ¹	\$707 ¹	\$1,800 ¹	\$1,800 ¹
Credit card sales (\$B) ¹	NA ¹	\$28 ¹	\$220 ¹	\$220 ¹
Credit card loans (\$B, EOP) ¹	\$142 ¹	\$131 ¹	\$211 ¹	\$233 ¹
Credit card loans market share ¹	19% ¹	17% ¹	17% ¹	17% ¹
Active credit card customers (M) ¹	NA ¹	561 ¹	571 ¹	571 ¹
# of branches ¹	2644 ¹	5,602 ¹	4,897 ¹	4,956 ¹
# of advisors ¹	NM ¹	3,900 ¹	5,456 ¹	5,755 ¹

Consumer & Community Banking

	2005	2014	2023	2024
Average deposits (\$B) ¹	\$887 ¹	\$487 ¹	\$1327 ¹	\$1064 ¹
Deposits market share ¹	4.5% ¹	7.9% ¹	11.4% ¹	11.3% ¹
# of top 50 markets where we are present ¹	6 (2) ¹	7 (2) ¹	22 (25) ¹	M (25) ¹
Business Banking primary market share ¹	4.0% ¹	7.2% ¹	9.5% ¹	9.7% ¹
Client investment assets (\$B) ¹	NA ¹	\$89 ¹	\$904 ¹	\$1,024 ¹
Total payments volume (\$T) ¹	NA ¹	\$16 ¹	\$59 ¹	\$65 ¹
% of digital non-card payments ¹	<20% ¹	49% ¹	79% ¹	81% ¹
Debt card sales (\$B)	NA ¹	\$40 ¹	\$194 ¹	\$204 ¹
Debt card sales (\$B)	NA ¹	\$241 ¹	\$551 ¹	\$546 ¹
Debt card sales volume (\$B) ¹	NA ¹	\$707 ¹	\$1,800 ¹	\$1,800 ¹
Credit card sales (\$B) ¹	NA ¹	\$28 ¹	\$220 ¹	\$220 ¹
Credit card loans (\$B, EOP) ¹	\$142 ¹	\$131 ¹	\$211 ¹	\$233 ¹
Credit card loans market share ¹	19% ¹	17% ¹	17% ¹	17% ¹
Active credit card customers (M) ¹	NA ¹	561 ¹	571 ¹	571 ¹
# of branches ¹	2644 ¹	5,602 ¹	4,897 ¹	4,956 ¹
# of advisors ¹	NM ¹	3,900 ¹	5,456 ¹	5,755 ¹

Commercial & Investment Banking

	2005	2014	2023	2024
Total Markets revenue ¹	NA ¹	#1 ¹	#1 ¹	#1 ¹
Market share ¹	6.5% ¹	8.7% ¹	11.2% ¹	11.4% ¹
Market share ¹	7.0% ¹	9.0% ¹	10.8% ¹	10.9% ¹
Equity ¹	#1 ¹	#1 ¹	#1 ¹	#1 ¹
Market share ¹	5.0% ¹	8.0% ¹	12.2% ¹	12.4% ¹
Global investment banking fees ¹	#2 ¹	#1 ¹	#1 ¹	#1 ¹
Market share ¹	5.0% ¹	8.0% ¹	12.2% ¹	12.4% ¹
Assets under custody (\$T) ¹	\$107 ¹	\$205 ¹	\$324 ¹	\$385 ¹
Average client deposits (\$B) ¹	\$220.8 ¹	\$612.4 ¹	\$929.2 ¹	\$961.4 ¹
Debt and capital markets (\$B) ¹	\$17.3 ¹	\$150.0 ¹	\$131.2 ¹	\$128.1 ¹
Payments revenue (\$B) ¹	\$4.9 ¹	\$19 ¹	\$113 ¹	\$184 ¹
Payments revenue (\$B) ¹	\$4.9 ¹	\$19 ¹	\$113 ¹	\$184 ¹
Total Markets revenue ¹	NA ¹	#1 (0.3%) ¹	#1 (0.5%) ¹	#1 (0.5%) ¹
# of top 75 MSAs with dedicated teams ¹	NA ¹	56 ¹	72 ¹	72 ¹
Average Banking & Payments loans (\$B) ¹	\$170 ¹	\$250 ¹	\$345.8 ¹	\$348.8 ¹
Average GCB & GIB Loans (\$B) ¹	\$32.0 ¹	\$123.5 ¹	\$202.2 ¹	\$220.0 ¹
Average GCB & GIB Loans (\$B) ¹	\$75.3 ¹	\$105.0 ¹	\$131.2 ¹	\$128.1 ¹
Multifamily lending ¹	#2 ¹	#1 ¹	#1 ¹	#1 ¹
# of GCB Bankers ¹	NA ¹	NA ¹	9,274 ¹	9,274 ¹
# of GCB Bankers ¹	NA ¹	NA ¹	3,469 ¹	3,700 ¹
# of GCB Bankers ¹	NA ¹	NA ¹	NA ¹	NA ¹
# of GIB Bankers ¹	NA ¹	NA ¹	NA ¹	NA ¹
# of GIB Bankers ¹	NA ¹	NA ¹	NA ¹	NA ¹

Commercial & Investment Banking

	2005	2014	2023	2024
Total Markets revenue ¹	NA ¹	#1 ¹	#1 ¹	#1 ¹
Market share ¹	6.5% ¹	8.7% ¹	11.2% ¹	11.4% ¹
Market share ¹	7.0% ¹	9.0% ¹	10.8% ¹	10.9% ¹
Market share ¹	5.0% ¹	8.0% ¹	12.2% ¹	12.4% ¹
Global investment banking fees ¹	#2 ¹	#1 ¹	#1 ¹	#1 ¹
Market share ¹	5.0% ¹	8.0% ¹	12.2% ¹	12.4% ¹
Assets under custody (\$T) ¹	\$107 ¹	\$205 ¹	\$324 ¹	\$385 ¹
Average client deposits (\$B) ¹	\$220.8 ¹	\$612.4 ¹	\$929.2 ¹	\$961.4 ¹
Debt and capital markets (\$B) ¹	\$17.3 ¹	\$150.0 ¹	\$131.2 ¹	\$128.1 ¹
Payments revenue (\$B) ¹	\$4.9 ¹	\$19 ¹	\$113 ¹	\$184 ¹
Payments revenue (\$B) ¹	\$4.9 ¹	\$19 ¹	\$113 ¹	\$184 ¹
Total Markets revenue ¹	NA ¹	#1 (0.3%) ¹	#1 (0.5%) ¹	#1 (0.5%) ¹
# of top 75 MSAs with dedicated teams ¹	NA ¹	56 ¹	72 ¹	72 ¹
Average Banking & Payments loans (\$B) ¹	\$170 ¹	\$250 ¹	\$345.8 ¹	\$348.8 ¹
Average GCB & GIB Loans (\$B) ¹	\$32.0 ¹	\$123.5 ¹	\$202.2 ¹	\$220.0 ¹
Average GCB & GIB Loans (\$B) ¹	\$75.3 ¹	\$105.0 ¹	\$131.2 ¹	\$128.1 ¹
Multifamily lending ¹	#2 ¹	#1 ¹	#1 ¹	#1 ¹
# of GCB Bankers ¹	NA ¹	NA ¹	9,274 ¹	9,274 ¹
# of GCB Bankers ¹	NA ¹	NA ¹	3,469 ¹	3,700 ¹
# of GCB Bankers ¹	NA ¹	NA ¹	NA ¹	NA ¹
# of GIB Bankers ¹	NA ¹	NA ¹	NA ¹	NA ¹
# of GIB Bankers ¹	NA ¹	NA ¹	NA ¹	NA ¹

Asset & Wealth Management

	2005	2014	2023	2024
JPMAM LT funds AUM performed above peer median (10-year) ¹	NA ¹	NA ¹	NA ¹	NA ¹
Client assets (\$T) ¹	\$311 ¹	\$2.3 ¹	\$5.0 ¹	\$5.5 ¹
Traditional assets (\$T) ¹	\$10 ¹	\$19 ¹	\$44 ¹	\$52 ¹
Equity ¹	\$20 ¹	\$24 ¹	\$30 ¹	\$35 ¹
Market share ¹	5.0% ¹	8.0% ¹	12.0% ¹	12.5% ¹
Global investment banking fees ¹	#2 ¹	#1 ¹	#1 ¹	#1 ¹
Market share ¹	5.0% ¹	8.0% ¹	12.0% ¹	12.5% ¹
Average deposits (\$B) ¹	\$42 ¹	\$146 ¹	\$216 ¹	\$235 ¹
Average loans (\$B) ¹	\$27 ¹	\$95 ¹	\$226 ¹	\$226 ¹
# of GCB Bank client advisors ¹	1484 ¹	2,392 ¹	3,915 ¹	3,770 ¹

Asset & Wealth Management

	2005	2014	2023	2024
JPMAM LT funds AUM performed above peer median (10-year) ¹	NA ¹	NA ¹	NA ¹	NA ¹
Client assets (\$T) ¹	\$311 ¹	\$2.3 ¹	\$5.0 ¹	\$5.5 ¹
Traditional assets (\$T) ¹	\$10 ¹	\$19 ¹	\$44 ¹	\$52 ¹
Equity ¹	\$20 ¹	\$24 ¹	\$30 ¹	\$35 ¹
Market share ¹	5.0% ¹	8.0% ¹	12.0% ¹	12.5% ¹
Global investment banking fees ¹	#2 ¹	#1 ¹	#1 ¹	#1 ¹
Market share ¹	5.0% ¹	8.0% ¹	12.0% ¹	12.5% ¹
Average deposits (\$B) ¹	\$42 ¹	\$146 ¹	\$216 ¹	\$235 ¹
Average loans (\$B) ¹	\$27 ¹	\$95 ¹	\$226 ¹	\$226 ¹
# of GCB Bank client advisors ¹	1484 ¹	2,392 ¹	3,915 ¹	3,770 ¹

Consumer & Community Banking

	2005	2014	2023	2024
Average deposits (\$B) ¹	\$887 ¹	\$487 ¹	\$1327 ¹	\$1064 ¹
Deposits market share ¹	4.5% ¹	7.9% ¹	11.4% ¹	11.3% ¹
# of top 50 markets where we are present ¹	6 (2) ¹	7 (2) ¹	22 (25) ¹	M (25) ¹
Business Banking primary market share ¹	4.0% ¹	7.2% ¹		

TO 00-25-203

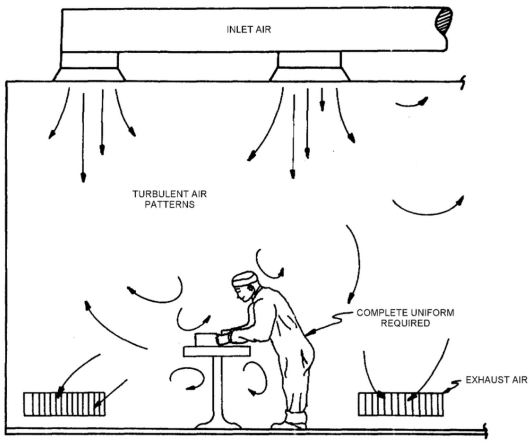


Figure 5-1. Typical Class 100,000, Clean Room Air Patterns

5.2.2.4 Pass Through Windows. Pass through windows or pass through boxes are small air locks through which hand tools or small parts can be transferred in or out of the clean room without carrying them through the larger air locks. They are for use during operating hours and will help minimize personnel traffic in and out of the clean room, and thus minimize the spread of contamination.

5.2.2.5 Clean Room. Clean rooms are restricted areas with limited access in which critical work is performed. Uniforms are required for all individuals entering. The rooms

are for the most part self-contained in that they incorporate all necessary power wiring, plumbing, vacuum systems, workbenches, vapor hoods, cleaning chambers, test equipment, furniture, part deli very systems, lighting and fixtures.

5.2.2.6 Office Space. Office space is provided as an uncontrolled area outside the clean room for routine paperwork. The supervisor's office is generally in the space, and windows are used to review the clean room.

5-2

TO 00-25-203

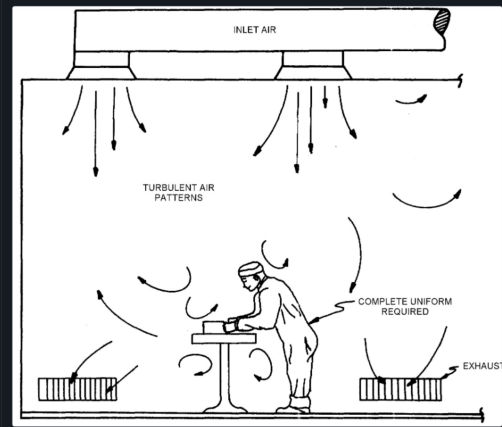


Figure 5-1. Typical Class 100,000, Clean Room Air Patterns

5.2.2.4 Pass Through Windows. Pass through windows or pass through boxes are small air locks through which hand tools or small parts can be transferred in or out of the clean room without carrying them through the larger air locks. They are for use during operating hours and will help minimize personnel traffic in and out of the clean room, and thus minimize the spread of contamination.

5.2.2.5 Clean Room. Clean rooms are restricted areas with limited access in which critical work is performed. Uniforms are required for all individuals entering. The rooms are for the most part self-contained in that they incorporate all necessary power wiring, plumbing, vacuum systems, workbenches, vapor hoods, cleaning chambers, test equipment, furniture, part deli very systems, lighting and fixtures.

5.2.2.6 Office Space. Office space is provided as an uncontrolled area outside the clean room for routine paperwork. The supervisor's office is generally in the space, and windows are used to review the clean room.

5-2

Figure 4: Example of bounding box generating models. Left: Original image. Right: Rendered transcription, with image crop corresponding to generated bounding box. Generated with LightOnOCR-2-1B-bbox.

Smarter, Better, Faster, Longer: A Modern Bidirectional Encoder for Fast, Memory Efficient, and Long Context Finetuning and Inference

Benjamin Warner^{1†} Antoine Chaffin^{2*} Benjamin Clavé^{1†}
 Orion Weller³ Oskar Hallström² Said Taghadouini²
 Alexis Gallagher¹ Raja Biswas¹ Faisal Ladha^{4*} Tom Aarsen⁵
 Nathan Cooper¹ Griffin Adams¹ Jeremy Howard¹ Iacopo Poli²

¹Answer.AI ²LightOn ³Johns Hopkins University ⁴NVIDIA ⁵HuggingFace

[†]: core authors, ^{*}: work done while at AnswerAI

Correspondence: {bw,bc}@answer.ai, antoine.chaffin@lighton.ai

Abstract

Encoder-only transformer models such as BERT offer a great performance-size tradeoff for retrieval and classification tasks with respect to larger decoder-only models. Despite being the workhorse of numerous production pipelines, there have been limited Pareto improvements to BERT since its release. In this paper, we introduce ModernBERT, bringing modern model optimizations to encoder-only models and representing a major Pareto improvement over older encoders. Trained on 2 trillion tokens with a native 8192 sequence length, ModernBERT models exhibit state-of-the-art results on a large pool of evaluations encompassing diverse classification tasks and both single and multi-vector retrieval on different domains (including code). In addition to strong downstream performance, ModernBERT is also the most speed and memory efficient encoder and is designed for inference on common GPUs.

1 Introduction

After the release of BERT (Devlin et al., 2019), encoder-only transformer-based (Vaswani et al., 2017) language models dominated most applications of modern Natural Language Processing (NLP). Despite the rising popularity of Large Language Models (LLMs) such as GPT (Radford et al., 2018, 2019; Brown et al., 2020), Llama (Touvron et al., 2023; Dubey et al., 2024), and Qwen (Bai et al., 2023; Yang et al., 2024), encoder-only models remain widely used in a variety of non-generative downstream applications.

The encoder’s popularity is largely due to their modest inference requirements, enabling them to efficiently process corpora of documents at scale for retrieval and quickly perform discriminative tasks. Encoder models offer a compelling trade-off in quality versus size, making them a popular

<https://github.com/AnswerDotAI/ModernBERT>

option against encoder-decoder and decoder-only language models when dealing with substantial amounts of data (Penedo et al., 2024).

Encoder models are particularly popular in Information Retrieval (IR) applications, e.g., semantic search, with notable progress leveraging encoders for this task (Karpukhin et al., 2020; Khatib and Zaharia, 2020). While LLMs have taken the spotlight in recent years, they have also motivated a renewed interest in encoder-only models for IR. Indeed, encoder-based semantic search is a core component of Retrieval-Augmented Generation (RAG) pipelines (Lewis et al., 2020), where encoder models are used to retrieve and feed LLMs with context relevant to user queries.

Encoder-only models are also still frequently used for a variety of discriminative tasks such as classification (Tunstall et al., 2022) or Natural Entity Recognition (NER) (Zarati et al., 2024), where they often match the performance of specialized LLMs. Here again, they can be used in conjunction with LLMs, for example detecting toxic prompts (Ji et al., 2023; Jiang et al., 2024b) and preventing responses, or routing queries in an agentic framework (Yao et al., 2023; Schick et al., 2023).

Surprisingly, these pipelines currently rely on older models, and quite often on the original BERT itself as their backbone (Wang et al., 2022; Xiao et al., 2023), without leveraging improvements developed in recent years. Practitioners face many drawbacks: sequence length limited to 512 tokens, suboptimal model design (Anthony et al., 2024) and vocabulary sizes (Karpathy, 2023), and generally inefficient architectures, whether in terms of downstream performance or computational efficiency. Finally, training data is limited in volume and restricted to narrow domains (especially lacking code data) or lacking knowledge of recent events.

Recent modernization efforts have only partially addressed the shortcomings of encoder-only mod-

Smarter, Better, Faster, Longer: A Modern Bidirectional Encoder for Fast, Memory Efficient, and Long Context Finetuning and Inference

Benjamin Warner^{1†} Antoine Chaffin^{2*} Benjamin Clavé^{1†}

Orion Weller³ Oskar Hallström² Said Taghadouini²

Alexis Gallagher¹ Raja Biswas¹ Faisal Ladha^{4*} Tom Aarsen⁵

Nathan Cooper¹ Griffin Adams¹ Jeremy Howard¹ Iacopo Poli²

¹ Answer.AI ² LightOn ³ Johns Hopkins University ⁴ NVIDIA ⁵ HuggingFace

[†] : core authors, ^{*} : work done while at AnswerAI

Correspondence: {bw,bc}@answer.ai, antoine.chaffin@lighton.ai

Abstract

Encoder-only transformer models such as BERT offer a great performance-size tradeoff for retrieval and classification tasks with respect to larger decoder-only models. Despite being the workhorse of numerous production pipelines, there have been limited Pareto improvements to BERT since its release. In this paper, we introduce ModernBERT bringing modern model optimizations to encoder-only models and representing a major Pareto improvement over older encoders. Trained on 2 trillion tokens with a native 8192 sequence length, ModernBERT models exhibit state-of-the-art results on a large pool of evaluations encompassing diverse classification tasks and both single and multi-vector retrieval on different domains (including code). In addition to strong downstream performance, ModernBERT is also the most speed and memory efficient encoder and is designed for inference on common GPUs.

1 Introduction

After the release of BERT (Devlin et al., 2019), encoder-only transformer-based (Vaswani et al., 2017) language models dominated most applications of modern Natural Language Processing (NLP). Despite the rising popularity of Large Language Models (LLMs) such as GPT (Radford et al., 2018, 2019; Brown et al., 2020), Llama (Touvron et al., 2023; Dubey et al., 2024), and Owen (Bai et al., 2023; Yang et al., 2024), encoder-only models remain widely used in a variety of non-generative downstream applications.

The encoder’s popularity is largely due to their modest inference requirements, enabling them to efficiently process corpora of documents at scale for retrieval and quickly perform discriminative tasks. Encoder models offer a compelling trade-off in quality versus size, making them a popular option against encoder-decoder and decoder-only language models when dealing with substantial amounts of data (Penedo et al., 2024).

Encoder models are particularly popular in Information Retrieval (IR) applications, e.g., semantic search, with notable progress on leveraging encoders for this task (Karpukhin et al., 2020; Khatib and Zaharia, 2020). While LLMs have taken the spotlight in recent years, they have also motivated a renewed interest in encoder-only models for IR. Indeed, encoder-based semantic search is a core component of Retrieval-Augmented Generation (RAG) pipelines (Lewis et al., 2020), where encoder models are used to retrieve and feed LLMs with context relevant to user queries.

Encoder-only models are also still frequently used for a variety of discriminative tasks such as classification (Tunstall et al., 2022) or Natural Entity Recognition (NER) (Zarati et al., 2024), where they often match the performance of specialized LLMs. Here again, they can be used in conjunction with LLMs, for example detecting toxic prompts (Ji et al., 2023; Jiang et al., 2024b) and preventing responses, or routing queries in an agentic framework (Yao et al., 2023; Schick et al., 2023).

Surprisingly, these pipelines currently rely on older models, and quite often on the original BERT itself as their backbone (Wong et al., 2022; Xiao et al., 2023), without leveraging improvements developed in recent years. Practitioners face many drawbacks: sequence length limited to 512 tokens, suboptimal model design (Anthony et al., 2024) and vocabulary sizes (Karpathy, 2023), and generally inefficient architectures, whether in terms of downstream performance or computational efficiency. Finally, training data is limited in volume and restricted to narrow domains (especially lacking code data) or lacking knowledge of recent events.

Recent modernization efforts have only partially addressed the shortcomings of encoder-only mod-

<https://github.com/AnswerDotAI/ModernBERT>

arXiv:2412.13663v2 [cs.CL] 19 Dec 2024

Figure 5: LightOnOCR-2-1B models excel at transcription of scientific documents. Left: Original image. Right: Rendered transcription. Generated with LightOnOCR-2-1B.

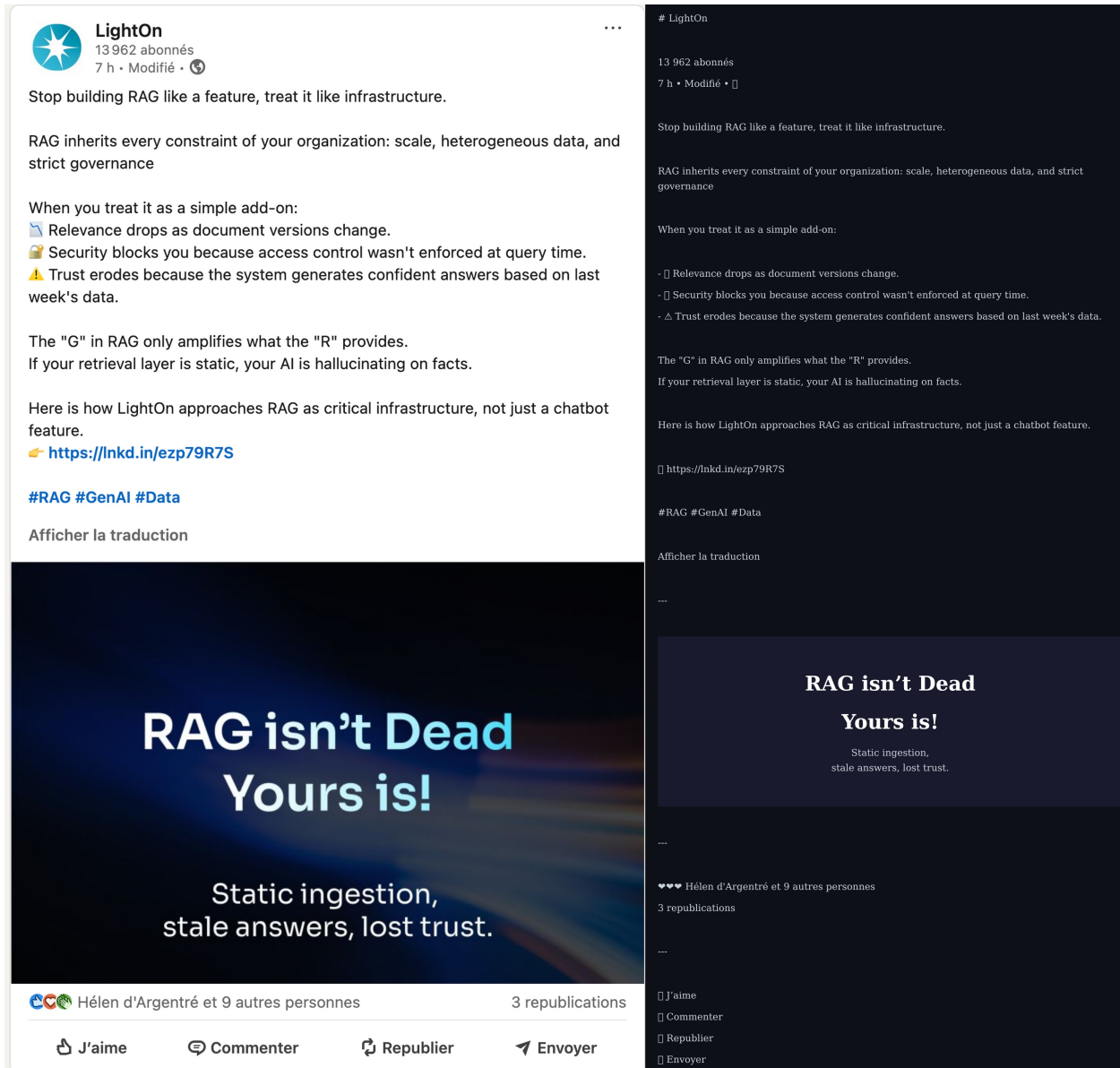


Figure 6: Example of transcription outside of distribution. Left: Original image. Right: Rendered transcription. Generated with LightOnOCR-2-1B.

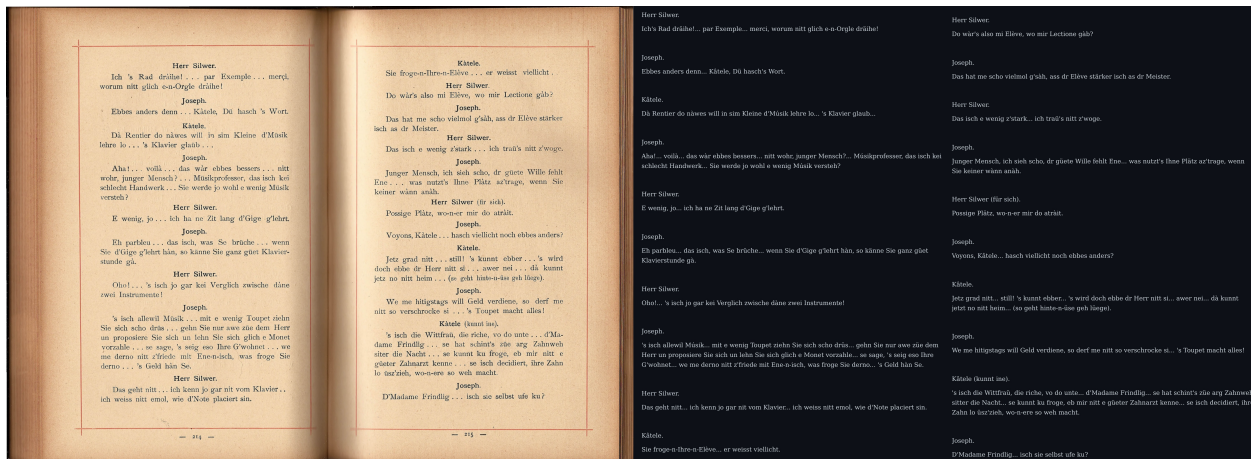


Figure 7: LightOnOCR-2-1B models were trained with a large portion of scanned documents which translates to improved performance on those types of files compared to v1. Left: Original image. Right: Rendered transcription. Generated with LightOnOCR-2-1B. Source: August Lustig, *Sämtliche Werke – Zweiter Band* (1909), p. 214–215. Wikimedia Commons, “ALustig_SämtlicheWerke_ZweiterBand_page214_215.pdf”, Public Domain (PDM 1.0)